applied sciences

MDPI

Article

Spraying of Viscous Liquids: Influence of Fluid-Mixing Mechanism on the Performance of Internal-Mixing Twin-Fluid Atomizers

Marek Mlkvik [1,*], Jan Jedelsky [2,†], Heike P. Karbstein [3,†] and Volker Gaukel [3,†]

1 Faculty of Mechanical Engineering, Slovak University of Technology in Bratislava, Nam. Slobody 17, 812 31 Bratislava, Slovakia
2 Faculty of Mechanical Engineering, Brno University of Technology, Technicka 2896/2, 616 69 Brno, Czech Republic; jedelsky@fme.vutbr.cz
3 Institute of Engineering in Life Sciences, Chair for Food Process Engineering, Karlsruhe Institute of Technology, Kaiserstrasse 12, 76131 Karlsruhe, Germany; heike.karbstein@kit.edu (H.P.K.); volker.gaukel@kit.edu (V.G.)
* Correspondence: marek.mlkvik@stuba.sk
† These authors contributed equally to this work.

Received: 6 July 2020; Accepted: 25 July 2020; Published: 30 July 2020

Abstract: The thermal usage of liquid fuels implies their combustion, which is a process strongly influenced by the performance of the atomizer, which disrupts the fuel into drops of the required sizes. The spray quality of the twin-fluid atomizers with internal mixing (IM-TFA) is primarily influenced by the two-phase flow pattern inside the mixing chamber. We studied the performance of the four types of the IM-TFA nozzles by the optical diffraction system (Malvern Spraytec) to answer the question of how the mixing chamber design influences the spray quality at low atomizing gas consumption. We tested the effervescent atomizer in outside-in-liquid (OIL) and outside-in-gas (OIG) configurations, the Y-jet nozzle and new nozzle design, and the CFT atomizer when spraying model liquids with the viscosities comparable to the common fuels (μ = 60 and 143 mPa·s). We found that the effervescent atomizer performance was strongly influenced by the configuration of the inlet ports. Although the OIL configuration provided the best spray quality (D_{32} = 72 µm), with the highest efficiency (0.16%), the OIG nozzle was characterized by unstable work and poor spray quality. Both the devices were sensitive to liquid viscosity. The Y-jet nozzle provided a stable performance over the liquid viscosity spectrum, but the spray quality and efficiency were lower than for the OIL nozzle. Our findings can be used to improve the performance of the common IM-TFA types or to design new atomizers. The results also provide an overview of the tested atomizers' performances over the wide range of working conditions and, thus, help to define the application potential of the tested nozzle designs.

Keywords: liquid atomization; twin-fluid nozzle; atomization efficiency; two-phase flows; spray quality

1. Introduction

The combustion of liquid fuels is a process of high industrial importance. Even when the number of oil-burning furnaces is continuously reduced due to environment protection reasons, it still takes place in furnaces in central heating systems or industrial furnaces. It is also the main energy source for gas turbines and internal combustion engines.

The term heating oil is a general designation of, mostly, petroleum products used for thermal usage, with viscosities within the range from approximately 2.5 mPa·s up to 360 mPa·s (at 40 °C).

The effective and environmentally friendly heating of oil-burning requires disruption of the fuel volume into small drops, which is a task fulfilled by the device called the atomizer or nozzle.

There are a variety of nozzles used in practical applications, but the twin-fluid atomizers with internal mixing of fluids (IM-TFA) have proven the capability to provide small drops with low energy consumption, even when spraying liquids of high viscosity, such as the marine diesel or heavy fuel oil [1–3]. The low energy consumption is explained by the fact that the IM-TFA provides a high-quality spray without the need to pressurize the liquid to a level as pressure nozzles need ($\approx 10^1$ to 10^2 MPa).

The typical application of IM-TFA is, except for combustion, the atomization of coke sludge slurries or liquid waste [1,3–5]. Other branches of industry where internal-mixing atomizers are commonly used are for example the pharmaceutical [6] or food-processing industry, where IM-TFA are used for atomization of different Newtonian and non-Newtonian liquids—water—oil emulsions [7,8], and gelatinized native corn starch [9]. Both the pharmaceutical and the food-processing industries also use spray-drying technology [10–12]. The ability to produce fine spray suitable for fire-suppression purposes serves as an alternative to the systems based on environmentally unfriendly and health-threatening HALON gas [13].

The work of IM-TFA is based on the creation of a two-phase flow inside the mixing chamber of the spraying device. The mixture flows through the mixing chamber until it reaches the discharge orifice [14]. The mixture discharge is a process where the intense gas-to-liquid interaction takes place. Liquid is accelerated and the energy of the expanding gas is used to shatter the liquid volume into smaller structures (ligaments) and finally into drops [1]. These processes are called primary and secondary liquid breakup.

The liquid-mixing and the two-phase flow development in the mixing chamber are the crucial processes of the IM-TFA work. The favourable internal flow pattern is an annular or wall-attached flow, leading to a stable liquid breakup and drops of uniform sizes [15,16]. The demand for efficient atomizer work requires a low gas consumption. A decrease of the gas content in the mixture supports the formation of slug or bubbly two-phase flow patterns, which downgrade the stability of the atomization and, consequently, the spray quality.

The mixing chamber flow pattern is the result of the viscous, gravitational, inertial forces and the surface tension equilibrium. The influence of individual forces on the flow in the mixing chamber can be described by the well-established dimensionless numbers—Weber (We_{mix}), Froude (Fr_{mix}), Ohnesorge (Oh_{mix}) and Bond number (Bo_{mix}). The two-phase flow pattern can be estimated by the two-phase flow maps which have been developed over past decades [17–19]. Regardless of the flow map used, the correct usage of this two-phase flow pattern estimation method requires a sufficiently long mixing chamber to allow the flow pattern to develop. This condition is hard to sustain in a real atomizer design. We will show that the above-mentioned flow maps do not provide sufficient internal flow description to explain the atomizers' behavior over the range of tested working conditions. An additional criterion, to estimate the internal Y-jet nozzle flow, was provided by [20]. The authors investigated the fluid injection into the mixing chamber and linked the ratio of the fluid momentum to the observed internal flow pattern. This approach was also successfully applied to the modified design of an effervescent atomizer [21,22].

The proper fuel combustion requires a certain spray quality, in the meaning of the provided drop sizes spectrum. The low sensitivity of the spray parameters on the liquid viscosity is also the advantageous capability of the well-designed atomizer.

Several internal-mixing atomizer designs have been proposed and studied in detail in past decades [12,21,23–25]. Unfortunately, there is a lack of papers oriented to the systematic comparison of different nozzles, which can help identify the key differences among nozzle types.

Some information can be found in [3,26], although these works are primarily oriented to the improvement of a specific atomizer type more than to the comparison of different nozzle designs. From recent research can be mentioned the work [10], where the authors compare the performance of the different nozzle designs according to energy consumption. The performance comparison of the

effervescent atomizer and the new type of internal-mixing atomizer, the ACLR nozzle, is provided in [27,28]. Here, the authors used statistical analysis to compare the spray quality of the two nozzle types.

The lack of published results oriented to the testing and comparison of different nozzle designs motivated us to perform experiments to answer the following questions: (1) What way nozzle design influences the fluid-mixing mechanism? (2) What is the effect of the fluid-mixing mechanism on the spray quality?

It is a known fact that the annular internal flow leads to good atomizer performance [15]. The spray quality worsens rapidly when internal flow changes to the plug or slug regime [10]. This fact contradicts to the requirement for efficient work, as the annular flow is usually linked with high gas content in the mixture.

Our present results document that even simple design difference between the OIG and OIL devices influences the internal flow significantly. We were able to achieve annular internal flow with the OIL device and good spray quality even with lowest gas consumption, while the performance of the OIG nozzle was poor at the same working regimes due to the plug/slug internal flows.

The influence of the mixing chamber design on internal flow and the spray quality is shown by the comparison of four atomizer types, some well-established and some experimental concepts. This research is a continuation of our previous work [21], where the liquid disintegration process of the same nozzles was compared using high- speed camera.

The Y-jet atomizer (Figure 1a), designed according to Mullinger and Chigier [29], is a well-known nozzle design, used in several industrial applications Ferreira et al. [3]. The internal flow of this device is created by injection of liquid into a high-speed gas stream. In contrast to this atomizer, the OIG and the OIL nozzles (Figure 1b) use fluid-mixing at low velocities. Both atomizers have the same design of their mechanical parts. The different atomizer performances were achieved by switching of the inlet ports into an "outside-in-gas" (OIG) or "outside-in-liquid" (OIL) configuration. The effervescent atomizer designed by the Lefebvre [30] represents the OIG configuration. As our previous work Mlkvik et al. [21] revealed, the investigated OIL configuration proved that the injection port configuration has a significant influence on the performance of the atomizer. This was later confirmed by Zaremba et al. [22]. The CFT (Figure 1c) nozzle has a design inspired by several previous works Chin [31], Ferreira M. Teixeira [32], Tamaki N.and Shimizu [33]. As opposed to the Y-jet nozzle, it is characterized by a low velocity of the internal flow. The mixing chamber is also significantly shorter than the mixing chamber of the OIG nozzle. This makes its design more compact and suitable for applications where a small atomizer body is required.

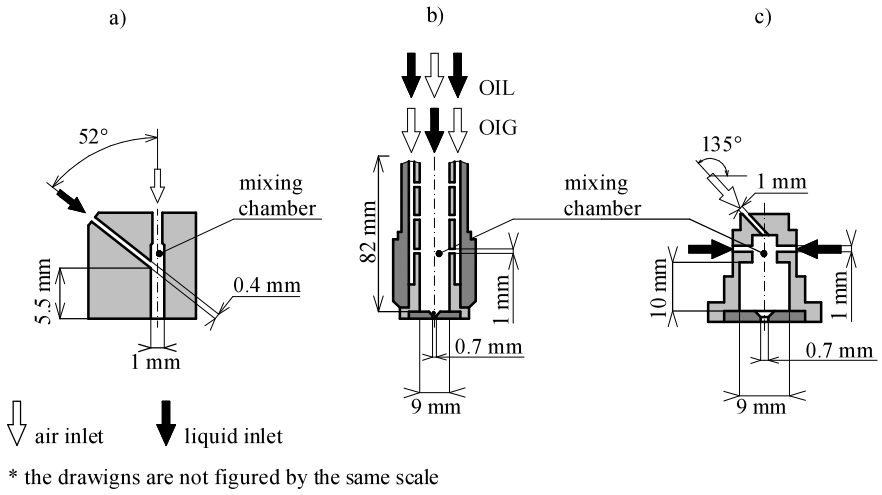

Figure 1. The atomizers geometry, (**a**) Y-jet atomizer, (**b**) OIL and OIG atomizers, (**c**) CFT nozzle.

2. Experiment and Methods

The experiments were conducted on the test bench schematically drawn in Figure 2. The pressurized vessel was used to drive the liquid into the atomizer and the liquid mass flow was controlled by a throttle valve. This approach was chosen to remove liquid flow variations caused by a pump. The air pressure in the mixing chamber was maintained by a pressure reduction valve. All the experiments were performed at air-conditioned room at temperature within the range 22–24 °C with 40% (liq. 1) and 45% (liq. 2) aqueous maltodextrin solutions (Table 1). Liquids were prepared at least 12 h before the tests and were stored in the same room, where the experiments were performed. Therefore, the room and the liquid temperatures were equalized. The physical properties of the maltodextrin solutions (Table 1) were taken from [10] and were measured at 25 °C (Table 1).

Table 1. Physical properties of the liquids.

liq. 1			liq. 2		
ρ [kg/m^3]	μ [mPa·s]	σ [n/m]	ρ [kg/m^3]	μ [mPa·s]	σ [N/m]
1185 ± 1	60 ± 4	74.54 ± 0.39	1121 ± 2	143 ± 16	74.26 ± 0.78

ρ-density, μ-viscosity, σ-surface tension.

The atomizer working regimes were defined by Δp = 0.14 MPa and with GLR within the range from 2.5 to 20% (Tables 2–5). We chose the inlet air pressure as an independent parameter because its contribution to the total energy balance dominates over the liquid inlet pressure [1]. Therefore, Δp can be related to the potential energy of the atomization process. The GLR was chosen because it is commonly used, and easy to measure, dimensionless parameter. As we did not experimentally investigate the internal flows, we used three different two-phase flow maps to estimate the internal flow structure: [17–19,34].

The internal flows were further described by a set of dimensional (gas and liquid superficial velocities (v_{gas} and v_{liq}), characteristic length scale of the internal flow structures (L)) and dimensionless criteria (Weber (We_{mix}), Bond (Bo_{mix}) and Froude (Fr_{mix})). The void fraction at the discharge orifice (α_{dis}) was estimated by a two-phase flow calculator [35].

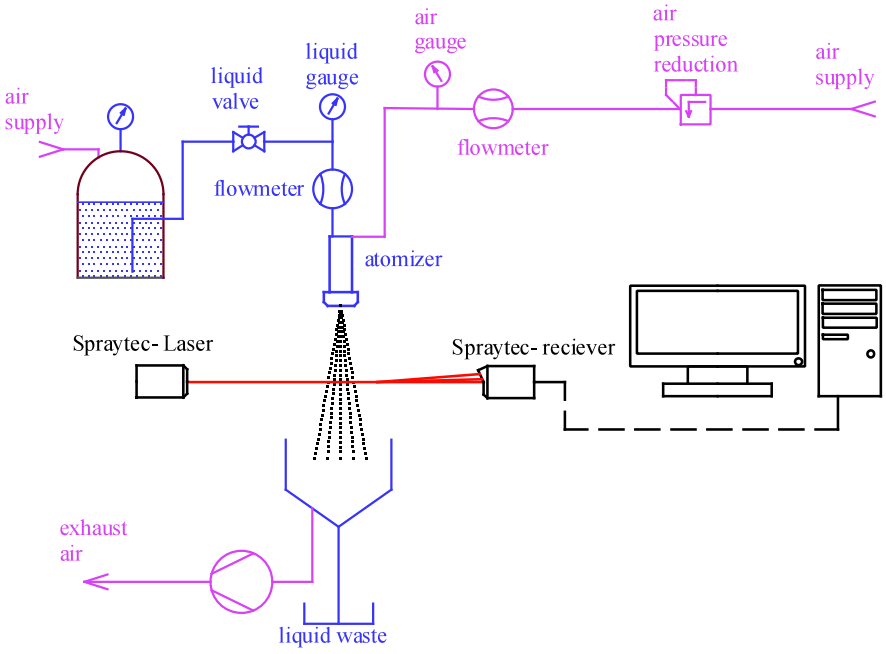

Figure 2. The test rig.

Table 2. Working parameters of the OIL nozle.

liq. 1 (40% Maltodextrin Solution)										
GLR	Q_{air} **[kg/h]**	Q_{liq} **[kg/h]**	v_{air} **[m/s]**	v_{liq} **[m/s]**	We_{mix}	L **[mm]**	Bo_{mix}	Fr_{mix}	Oh_{mix}	α_{dis} **[%]**
2.5	0.10	3.79	0.148	0.014	2.6	3.5	1.92	0.75	0.11	0.91
5.0	0.14	2.73	0.207	0.010	5.5	1.6	0.41	1.56	0.16	0.95
10.0	0.19	1.90	0.296	0.007	11.9	0.8	0.09	3.35	0.23	0.98
20.0	0.21	1.07	0.326	0.004	14.7	0.6	0.06	4.16	0.26	0.99
liq. 2 (45% Maltodextrin Solution)										
2.5	0.10	3.59	0.153	0.014	2.6	3.5	1.77	4.07	0.27	0.92
5.0	0.14	2.47	0.207	0.010	5.3	1.7	0.43	11.77	0.39	0.96
10.0	0.16	1.43	0.237	0.006	7.2	1.3	0.23	18.85	0.45	0.98
20	0.19	0.90	0.296	0.003	11.5	0.8	0.09	38.17	0.57	0.99

Table 3. Working parameters of the Y-jet nozle.

liq. 1 (40% Maltodextrin Solution)										
GLR	Q_{air} **[kg/h]**	Q_{liq} **[kg/h]**	v_{air} **[m/s]**	v_{liq} **[m/s]**	We_{mix}	L **[mm]**	Bo_{mix}	Fr_{mix}	Oh_{mix}	α_{dis} **[%]**
2.5	0.078	3.081	19.579	1.877	8.4	0.084	0.00108	617.90	0.70	0.91
5.0	0.136	2.726	34.264	1.660	28.4	0.025	0.00009	2095.80	1.28	0.95
10.0	0.194	1.896	48.948	1.155	61.0	0.011	0.00002	4503.51	1.88	0.98
20.0	0.233	1.126	58.738	0.686	90.0	0.008	0.00001	6644.34	2.28	0.99
liq. 2 (45% Maltodextrin Solution)										
2.5	0.06	2.19	14.684	1.407	4.7	0.149	0.00324	347.55	1.28	0.91
5.0	0.08	1.57	19.579	1.011	9.2	0.076	0.00085	679.80	1.79	0.95
10.0	0.12	1.23	29.369	0.794	21.8	0.032	0.00015	1609.85	2.75	0.97
20.0	0.17	0.84	44.053	0.541	50.5	0.014	0.00003	3732.80	4.19	0.99

Table 4. Working parameters of the OIG nozle.

liq.1 (40% Maltodextrin Solution)										
GLR	Q_{air} **[kg/h]**	Q_{liq} **[kg/h]**	v_{air} **[m/s]**	v_{liq} **[m/s]**	We_{mix}	L **[mm]**	Bo_{mix}	Fr_{mix}	Oh_{mix}	α_{dis} **[%]**
2.5	0.10	4.03	0.149	0.015	2.5	3.5	1.94	0.52	0.11	0.91
5.0	0.14	2.73	0.208	0.010	5.6	1.6	0.40	2.47	0.16	0.95
10.0	0.19	1.96	0.297	0.007	12.0	0.8	0.09	11.38	0.23	0.98
20.0	0.21	1.07	0.327	0.004	14.8	0.6	0.06	17.52	0.26	0.99
liq.2 (45% Maltodextrin Solution)										
2.5	-	-	-	-	-	-	-	-	-	-
5.0	0.14	2.47	0.207	0.010	5.3	1.7	0.43	2.33	0.38	0.96
10.0	0.17	1.57	0.266	0.006	9.1	1.0	0.14	7.00	0.51	0.98
20.0	0.19	0.90	0.296	0.003	11.5	0.8	0.09	11.17	0.57	0.99

Table 5. Working parameters of the CFT nozle.

Liq. 1 (40% Maltodextrin Solution)										
GLR	Q_{air} **[kg/h]**	Q_{liq} **[kg/h]**	v_{air} **[m/s]**	v_{liq} **[m/s]**	We_{mix}	L **[mm]**	Bo_{mix}	Fr_{mix}	Oh_{mix}	α_{dis} **[%]**
2.5	0.12	4.74	0.178	0.017	0.075	3.7	2.4	0.93	0.13	1.08
5.0	0.17	3.32	0.267	0.012	0.075	9.3	1.0	0.15	0.20	6.83
10.0	0.19	1.96	0.297	0.007	0.075	12.0	0.8	0.09	0.23	11.38
20.0	0.23	1.13	0.357	0.004	0.075	17.7	0.5	0.04	0.28	24.85
Liq. 2 (45% Maltodextrin Solution)										
2.5	-	-	-	-	-	-	-	-	-	
5.0	0.14	2.47	0.208	0.010	0.075	5.3	1.7	0.42	0.38	2.36
10.0	0.12	1.23	0.178	0.005	0.075	4.0	2.2	0.72	0.38	1.38
20.0	0.14	0.67	0.208	0.003	0.075	5.7	1.6	0.37	0.39	2.71

Instantaneous drop sizes ($D_{32,t.d.}$) were measured by the laser diffraction system (Malvern Spraytec) at a distance 100 mm downstream to the discharge orifice. The measurement distance

was theoretically estimated according to [36]. The calculations were done by presumption that the liquid exits the atomizers in the form of a thin film. The input data of the calculations were taken from our previously published results [21], which dealt with the observations of the liquid discharge in the close distance from the exit orifice. The longest theoretically estimated breakup distance was 40 mm for the Y-jet nozzle working with the more viscous liquid at GLR = 2.5%. The liquid breakup distance for the other nozzles was estimated within the range from 7 to 8 mm. The distance 100 mm between the nozzle and the drop size measurement site was, therefore, considered to be sufficient to avoid the presence of the ligaments. This consideration was further verified by direct observation of the spray pattern at the drop sizes measurement site by high-speed camera. The presence of the ligaments was not observed for any of the tested operating regimes of the nozzles, except for the ones where the nozzles did not atomize the liquid. The sample image of the spray pattern, as observed in the drop sizes measurement site, is shown in Figure 3. The measurement frequency was 500 Hz and the measurement period was 25 s. The time-averaged Sauter mean diameters (D_{32}) were then estimated as the arithmetic means of the recorded 12,500 samples of $D_{32,t.d.}$ values.

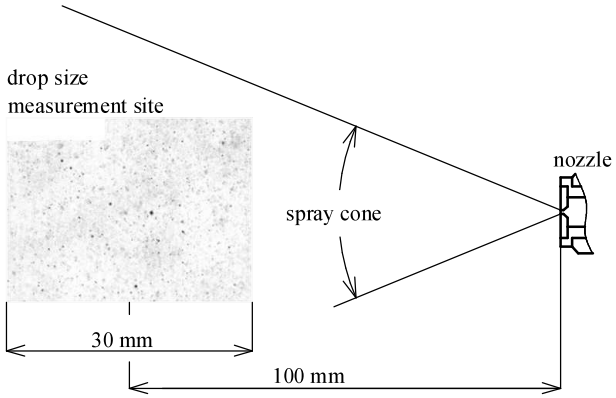

Figure 3. The spray pattern without non-spherical objects, required to perform measurements with Malvern Spraytec device. Image taken for Y-jet nozzle at GLR = 2.5% (liq. 2) with OLYMPUS i-speed2 camera.

The standard deviation (STD_{D32}) was used to measure the drop sizes variations of the measured dataset. As previously shown in Kleinhans et al. [27], this method can identify the pulsations, but can lead to incorrect assumptions about the atomization process. To study the atomizers work, were involved two methods of the time-resolved analysis of the drop sizes. The first method was the conversion of the time-dependent data ($D_{32,t.d.}$) into the Cumulative Distribution Function (CDF). This approach allowed us to analyze the whole range of the measured $D_{32,t.d.}$ and in this way to identify the spray pulsations. The second method, the FFT (Fast Fourier Transform) analysis, was used to identify the periodic behavior of the spray pulsations and to indirectly gain information about the two-phase flow in the atomizer mixing chamber. Similar analysis was, for the numerical simulation results, used in [37].

The economy of the atomizer work was estimated in two ways. The atomization efficiency (η) and its sensitivity to the liquid viscosity are related to the process of liquid breakup and drops formation. The efficiency was calculated according to Jedelsky and Jicha [1] as a ratio of the surface tension energy of drops in the spray (E_a), to the total energy (E_1) required to produce the spray ($\eta = \frac{E_a}{E_1}$).

3. Time-Averaged Spray Analysis

The unstable atomizer performance was characterized by the spray cone pulsations, followed by the formation of the various drop sizes. In this section, we analyze the uniformity of the size

distributions of the generated drops by the standard deviation of the time-averaged D_{32} (denoted in Figure 3 by the error bars).

The expected trend, an increase in drop sizes with reducing GLR, was observed for all the investigated cases. Also, D_{32} was comparable for all the tested devices for GLR $\geq$ 10%. As atomization with low gas consumption is the key advantage of internal-mixing devices in comparison to their external mixing counterparts, we focused our further analysis on regimes with GLR $\leq$ 5%.

The OIL atomizer generally produced the smallest drops from among all the tested devices. It also atomized both liquids under the whole range of investigated GLRs. The drops with D_{32} = 130 µm were produced with the more viscous liquid at GLR = 2.5%. For liquid with lower viscosity the drops were smaller (75 µm). Similar sensitivity of the D_{32} to the liquid viscosity was, observed for all the GLRs with this atomizer. On the other hand, low pulsations for almost all the investigated regimes were typical for the OIL device. The only significant error bar ($\pm$26 µm) is present for the GLR = 2.5% and liquid viscosity μ_l = 143 mPa·s.

The OIG atomizer, however, has the same design as the previously mentioned device but provided considerably worse performance. It did not atomize the liq. 2 at GLR = 2.5%, and it produced D_{32} larger than 300 µm at GLR = 5% with this liquid. For some applications, this can be considered, as unacceptable result. This device also shows sensitivity to μ_l. It atomized the second, less viscous, liquid across the whole GLR range with acceptable drop sizes of 102 and 70 µm at the GLR = 2.5 and 5% respectively. The D_{32} was not the only qualitative parameter which got worse when the OIG atomizer was used instead of its OIL counterpart. The error bars in Figure 4, indicate that at low GLRs, the OIG device produced a spray with varying drop sizes, which can be related to the plug/slug internal two-phase flow pattern previously estimated in [21]. The most intense pulsations were present when liquid liq. 2 was atomized, causing a very broad error bar at GLR = 5%.

The low sensitivity of the generated spray quality to the liquid viscosity (for the corresponding GLRs) was characteristic of the Y-jet atomizer. For GLR = 2.5%, the drops had sizes of 130 and 150 µm for liq. 1 and liq. 2, respectively. At GLR = 5% the average drop size for both liquids was 80 µm. The spray pulsations (characterized by the D_{32} error bars) were most intense at lowest GLR and were comparable for both liquids ($STD_{D32} \approx$ 15 µm). This is an important difference in comparison to the previously discussed devices, where spray pulsations intensity, as well as drop size, depended on liquid viscosity.

The last of the tested devices, the CFT atomizer, produced at low GLRs the spray with the largest drops among the set of the tested devices. As with the OIG device, the CFD nozzle did not atomize the more viscous liquid at GLR = 2.5%. The error bars of the D_{32} indicates that the drops size spectrum was comparable for the two liquids, except for GLR = 2.5%, where the comparison could not be done.

The time-averaged analysis provided us with some spray quality comparisons. Increasing STD_{D32} for low GLRs indicated unstable atomizer operation, but did not allow us to study the spray dynamic behavior. Accordingly, time-dependent analyses were used to study in detail drop size distributions and spray pulsations.

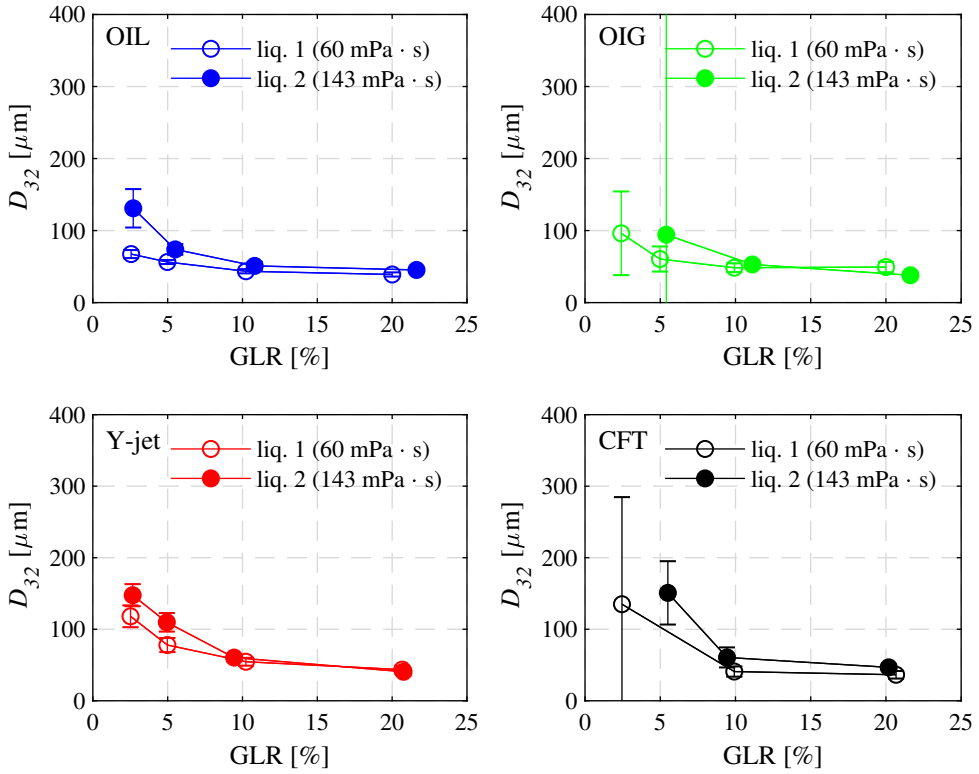

Figure 4. Time-averaged drop sizes.

4. Time-Resolved Spray Behavior

Figure 5, provides the first insight into the temporal spray behavior. Although the stable drop sizes were characteristic of a high GLR regime for the given example (CFT atomizer), the $D_{32,t.d.}$ was fluctuating at GLR = 2.5%. To quantify the drop size fluctuations, the time-dependent drop sizes were analyzed by converting the recorded $D_{32,t.d.}$ into the Cumulative Distribution Function (CDF). The y-axis of the Figure 4 (right) represents the equally divided classes of drop sizes. The CDF is plotted within the range from 0 to 1 on the x-axis. The axis configuration in Figure 4, however not typical for CDF, was chosen to show the relation of the recorded time-dependent data and processed results.

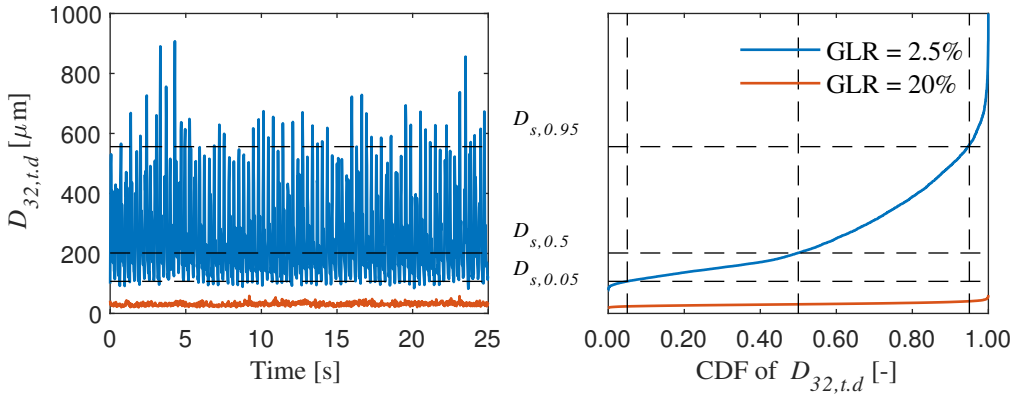

Figure 5. The drop sizes plotted vs. time (**left**) and converted into CDF (**right**) for the CFT nozzle spraying the less viscous liquid.

The stable regimes led to a narrow CDF, while CDF for the pulsating regimes was broad due to the wide spectrum of the drop sizes in the measured sample. Depicted values ($D_{S,0.05}$, $D_{S,0.5}$, $D_{S,0.95}$) represent the 5th, 50th (median) and 95th percentile of the CDF of $D_{32,t.d.}$. The time-dependent data were further converted into power spectra (using the Fast Fourier Transform–FFT) to investigate the periodic spray behavior (Figure 6).

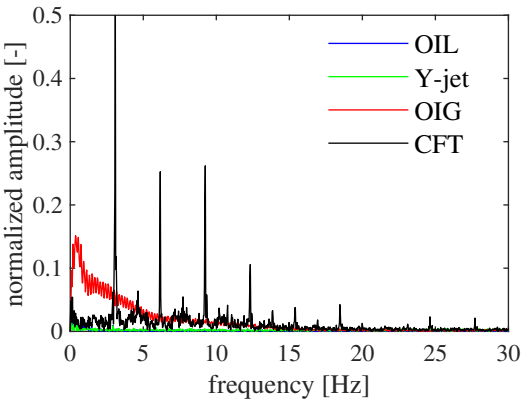

Figure 6. Power spectra of the $D_{32t.d.}$ at GLR = 2.5%, μ_l = 60 mPa·s.

4.1. Spraying at Low GLR

With regard to the values of We_{mix}, Bo_{mix} and the Fr_{mix} (Table 2), the OIL device was characterized by the dominant influence of fluid inertia and gravity on the internal flow. The internal flow pattern was identified as the wall-attached [16,21,22], Figure 7a). The internal two-phase flow pattern led to the continuous passage of the liquid film through the discharge orifice without significant GLR fluctuations [15]. The resultant spray was produced with low drop sizes variations: 95% of all the drops were smaller than 84.8 µm. The overall spray quality was underlined by the maximum measured drop size D_{max} = 97.1 µm (Table 6), which was just 14% larger than the $D_{S,0.95}$ value. Therefore, even the largest drops were of acceptable size. The increase in liquid viscosity to 143 mPa·s caused, under the same working conditions, a decrease in spray quality. Although most of the drops were of the sizes 98.7 to 166.5 µm, the spray also contained drops as large as 656.9 µm. It was observed that the change in viscosity led to an increase of the Oh_{mix} from 0.11 to 0.27 (Table 2). Both values are very low and point to a low influence of the viscous forces on the internal flow, but the relative Oh_{mix} increase is high (150%). As the Ohnesorge number influences liquid deformation time [38], we can assume that the internal flow did not fully develop with the more viscous liquid.

The dimensionless parameters of the Y-jet nozzle internal flow indicate the low influence of gravitational forces on the two-phase flow pattern (the low value of Bo_{mix}) and the importance of the fluid inertia, documented by the We_{mix} = 8, which resulted from small mixing chamber dimensions and the large gas-to-liquid velocity difference (Table 3). It was previously determined [21] that most of the injected liquid penetrates the high-velocity gas stream and reaches the opposite wall, continuing to flow downstream to the discharge, while a portion of the liquid detaches from the liquid stream and creates liquid drops of random sizes inside the mixing chamber Figure 7). The result of the above-described mixture discharge was a spray with $D_{S,0.05}$ to $D_{S,0.95}$ range within 99.5 and 150 µm and a drop median size 122 µm (Figure 8, Table 6). The largest drops were of 213 µm, which is acceptable in applications where the drop size is not the main qualitative criterion. According to the relatively high value of the Oh_{mix} (0.7 (liq. 1) and 1.28 (liq. 2)), compared to the other investigated devices, we could expect sensitivity of the Y-jet nozzle performance to the liquid viscosity. However, the opposite was true. We observed that while the absolute values of the Oh_{mix} are high, the relative change of the Ohnesorge number is small (82%), in comparison to the other tested devices (typically about 150–250%). Therefore, the work of the Y-jet atomizer was less influenced by the liquid used.

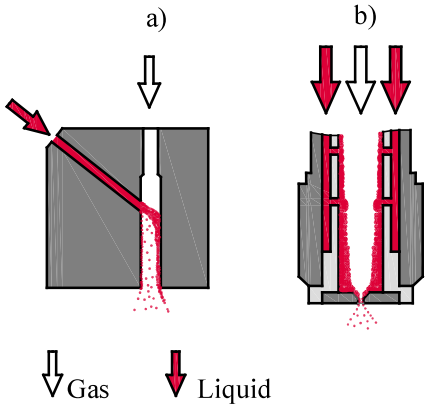

Figure 7. Internal two-phase flow patterns estimated for the Y-jet (**a**) and the OIL atomizer (**b**).

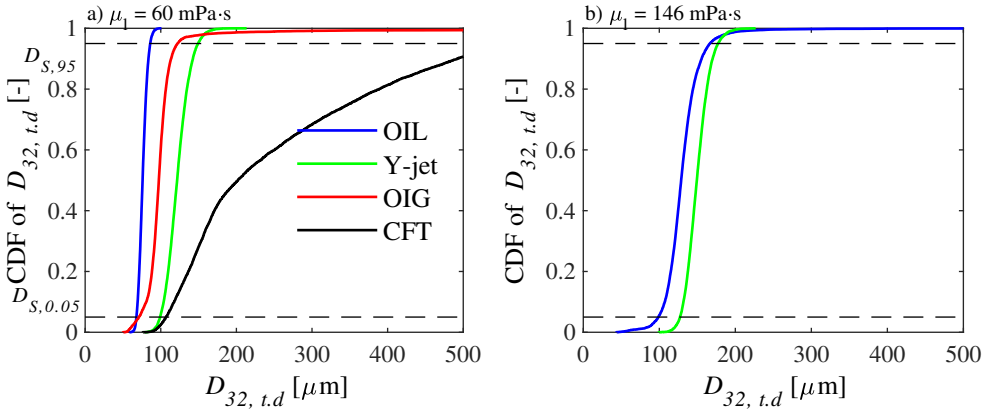

Figure 8. CDF of time-dependent drop sizes for spraying at GLR = 2.5%.

Table 6. Parameters of the spray drop size distribution at $GLR = 2.5\%$.

			liq. 1		
Atomizer	D_{min}	$D_{S,0.05}$	$D_{S,0.5}$	$D_{S,0.95}$	D_{max}
OIL	60.3	63.6	75.4	84.8	97.1
Y-jet	78.7	99.5	122.1	150.0	213.5
OIG	50.1	71.1	97.4	122.1	1409.6
CFT	99.27	126.7	149.7	562.1	1080.7
			liq. 2		
OIL	45.6	98.7	128.8	166.5	656.9
Y-jet	99.3	127.3	149.4	177.3	226.8

The OIG (effervescent) atomizer shows the influence of the mixing of the fluids on the internal flow. All the internal flow dimensionless parameters of this device were comparable to its OIL counterpart, and yet, the OIL and the OIG performance differed sharply. The switch of the gas and liquid injection ports led to an internal flow different from those observed for the OIL nozzle [16,22]. Two-phase flow maps are often used to determine the internal flow pattern for the OIG type of atomizers [1,39]. We applied three flow maps to estimate the internal flow pattern for the OIG device (Table 7). The results show a disagreement between the flow maps in the two-phase flow pattern estimation. In particular, the map provided by [18] estimated an annular flow which is in contradiction with the other two-phase flow maps as well as with the experimental results. Figure 8 shows that most of the produced drops were of the size within the $D_{S,0.05}$ to $D_{S,0.95}$ interval from 71.1 to 122.1 µm. The spray quality was lowered by the presence of a drops with D_{max} as large as 1400 µm, which points to unstable conditions at discharge, typical for the plug flow [15]. The shape of the power

spectrum (Figure 6) was characteristic for the stochastic signal. When the plug flow occurs in the mixing chamber (Figure 9), the ratio of the gas and liquid mass flows in the discharge orifice randomly varies, due to the passage of the large bubbles (plugs) alternated by the flow of the liquid without gas content. The variation of the discharged mixture composition is the source of the variations of the liquid breakup conditions in the near nozzle area of the atomizer which leads to the production of the wide spectrum of the drop sizes. We presume that the largest drops originated from the occasional discharge of a large amount of liquid not well mixed with the atomizing gas as the result of the internal plug/slug two-phase flow pattern. The above-described behavior should be considered when using the OIG atomizer, especially in applications such as spray-drying, where the large drops cannot be dried quickly enough. These drops can hit the hot wall, burn and contaminate the spray dryer with smoke. When liquid viscosity raised to 143 mPa·s, the OIG device did not atomize the liquid. The non-atomized liquid was ejected from the discharge orifice (Figure 10a) followed by the expansion of a pressurized gas (Figure 10b) with low liquid content. This indicates an internal flow with insufficient mixing, leading to separate gas and liquid volumes being discharged without proper liquid atomization. Similar observations were previously provided by [27].

Table 7. Estimation of the OIG atomizer internal flows by different two-phase flow maps at GLR = 2.5%.

		liq.1	
GLR	**Baker-Modified (1964)**	**Golan and Stenning (1969)**	**Barnea (1987)**
2.5	Plug/Slug	annular mist/annular flow	elongated bubbles
5.0	Plug/Slug	annular mist/annular flow	elongated bubbles
10.0	Plug/Slug	annular mist/annular flow	elongated bubbles
20.0	Plug/Slug	annular mist/annular flow	annular
		liq.2	
2.5	-	-	-
5.0	Plug/Slug	annular mist/annular flow	elongated bubbles
10.0	Plug/Slug	annular mist/annular flow	elongated bubbles
20.0	Plug/Slug	annular mist/annular flow	elongated bubbles

At the GLR = 2.5%, the CFT nozzle provided the worst overall results, despite the fact that the dimensionless parameters (Table 5), as well as the two-phase flow maps [16,21], indicated internal flow conditions similar to the OIG nozzle. The only geometrical parameter not involved in our dimensionless analysis was the mixing chamber length. We can, therefore, presume that the CFT nozzle mixing chamber was not long enough for a two-phase flow to develop. As a result, the spray is characterized by drops with non-uniform drop sizes, with the largest drops reaching the size of 1080 µm in diameter. Moreover, the more viscous liquid was not atomized at all and the CFT atomizer provided behavior similar to the OIG device (Figure 10a,b).

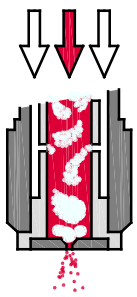

Figure 9. Internal plug flow pattern estimated for the OIG atomizer at GLR = 2.5%, μ_l = 60 mPa·s.

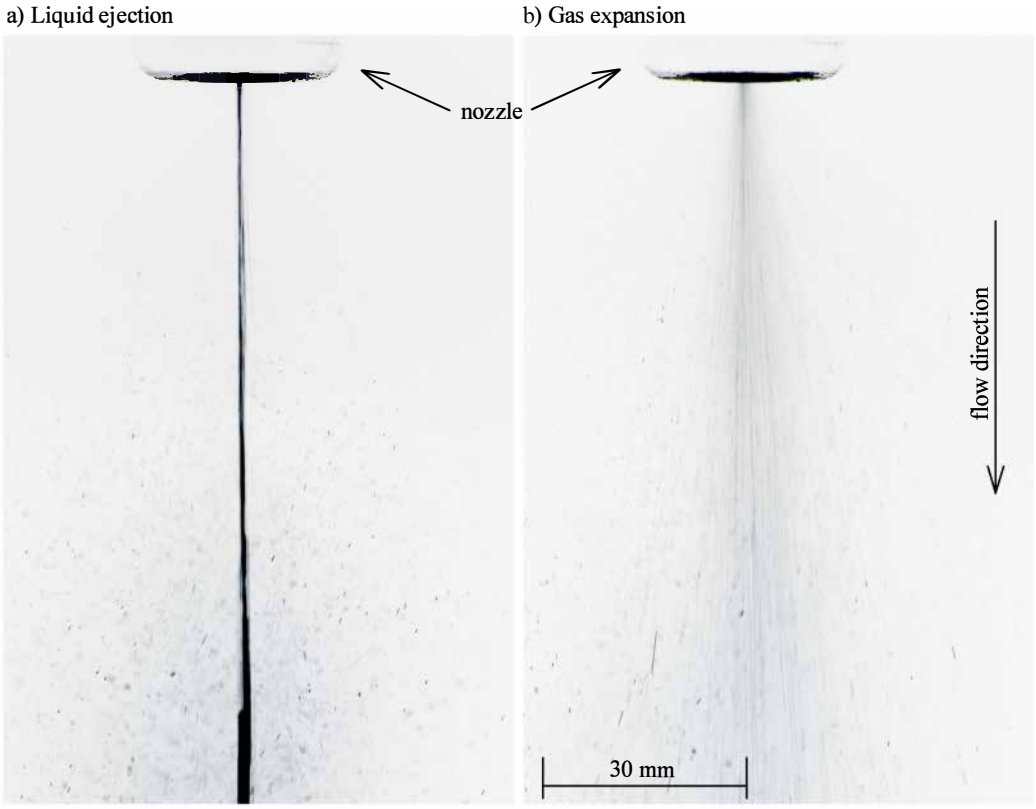

Figure 10. Example of the viscous liquid spraying by the CFT atomizer at GLR = 2.5% (similar spray patterns were observed for the OIG atomizer under the same working conditions).

4.2. Spraying at High GLRs

The increased gas consumption at GLR = 5% consequently led to a discharge void fraction increase of up to 95% for all the devices. As the atomizing energy increased ([1]), all the devices produced a spray of higher quality in comparison to the low-GLR regime.

The internal flows of all the atomizers were mainly influenced by the fluid inertial forces (Tables 2–5).

The best performance with both liquids is provided by the OIL atomizer. This device's work was characterized by low drop size oscillations, as documented by the flat power spectrum (Figure 11) and the narrow CDF curve (Figure 12).

The Y-jet nozzle provided a spray with median drop sizes $D_{S,0.5}$ = 79.8 and 84.2 μm with liq. 1 and liq. 2, respectively. The internal flow pattern did not change with the increased gas consumption [21], so the CDFs for both liquids indicate low spray pulsations (Table 8, Figures 11 and 12).

OIG device spraying with the less viscous liquid is characterized by a narrow drop size spectrum with a median drop size of 66.9 μm. In comparison to the low-GLR regime, the spray quality improvement lies in the fact that no extremely large drops were detected. This implies a change in the internal flow pattern. The increase of the We_{mix} led to a reduction in the characteristic length (L) of the gas structures in the mixing chamber. It is important to mention that none of the flow maps used (Table 7) predicted this fact. Except for the Ohnesorge number, the liquid viscosity increase did not influence the dimensionless parameters of the OIG nozzle internal flow.

As the Oh_{mix} raised, the influence of viscosity on the flow become significant. Under these conditions, intense random gas and liquid bursts occurred (Figure 11b), followed by the production of a wide drop sizes spectrum (Figure 12b).

Table 8. Parameters of the spray drop size distribution at $GLR = 5\%$.

Atomizer	D_{min}	$D_{S,0.05}$	$D_{S,0.5}$	$D_{S,0.95}$	D_{max}
			liq. 1		
OIL	44.2	48.5	52.6	57.6	67.5
Y-jet	53.6	66.6	79.8	98.6	148.3
OIG	38.4	47.4	66.9	100.8	158.3
CFT	47.3	69.4	98.16	191.0	684.91
			liq. 2		
OIL	49.1	59.1	69.2	83.4	114.5
Y-jet	53.8	68.4	84.2	110.2	199.3
OIG	27.5	44.5	92.3	1086.0	1557.0
CFT	71.0	96.2	138.6	233.0	330.61

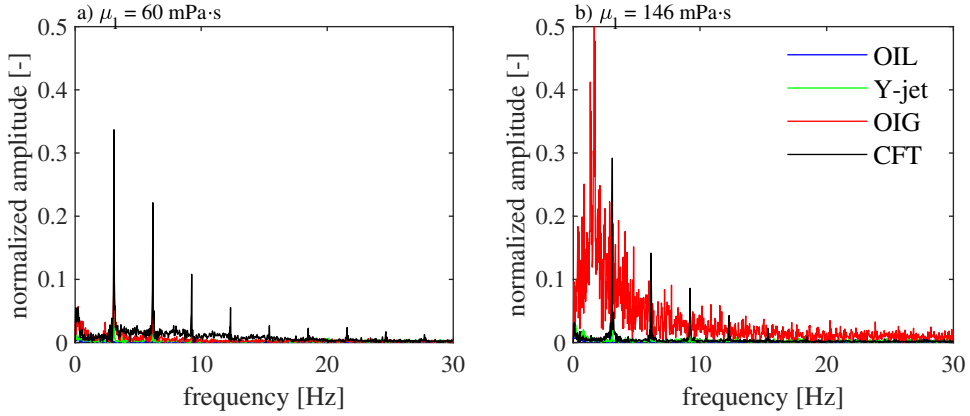

Figure 11. Power spectra of time-dependent drop sizes for spraying at GLR = 5%.

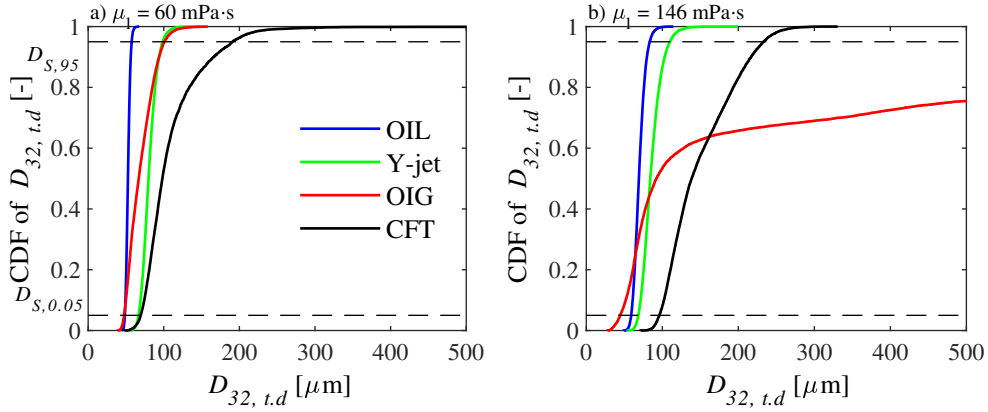

Figure 12. CDF of time-dependent drop sizes for spraying at GLR = 5%.

5. Atomization Efficiency

Although drop size is an important marker of spray quality, atomization efficiency is relevant for an evaluation of the energy consumption of the entire technological process (combustion, spray-drying and others). The relation of the atomization efficiency and spray quality is plotted in Figure 13. It shows the known dependency of the D_{32}: smaller drops are produced with lower efficiency. The physical explanation of this trend can be found in previous works [1,10]. We will, therefore, focus only on the comparison of the nozzles.

Small drops (<60 µm) were produced with efficiency from 0.03 to 0.06% by all the atomizers, regardless of the liquid used. This drop size range was related to high GLR regimes (GLR > 5%) where the spraying process was characterized by stable spray production. The significant difference

in the atomization efficiency was found at lower GLRs, characterized by the production of larger drops. The differences among the atomizers is shown on two parameters: atomization efficiency and its sensitivity to liquid viscosity at low GLRs.

When the less viscous liquid was sprayed, the best overall results were observed for the OIL nozzle (Figure 13). It reached 0.16% efficiency for the D_{32} = 75 µm. The other atomizing devices reached this spray quality with much lower efficiencies— less than 0.1%.

The Y-jet atomizer was typified by the stable spray production, with efficiency comparable to the OIG and the CFT nozzles.

At low GLRs, the viscosity increase to 143 mPa·s led to a less efficient spraying process for all the tested devices. The lowest efficiency was recorded with the OIG and the CFT nozzles. Both devices produced averaged drop sizes 100 µm with $\eta \approx 0.05\%$. The highest sensitivity of η to liquid viscosity was shown by the OIL atomizer. However, at the lowest GLR with liq. 2, this device provided the smallest drops (135 µm) with the highest efficiency (0.08%) among the tested atomizers; the relative decrease of the η with liquid change was the most significant. On the other hand, when spraying the more viscous solution the Y-jet atomizer showed the lowest relative decrease of efficiency, which is in accordance with the fact that the spray stability of this device (for corresponding GLRs) was not significantly influenced by liquid physical properties.

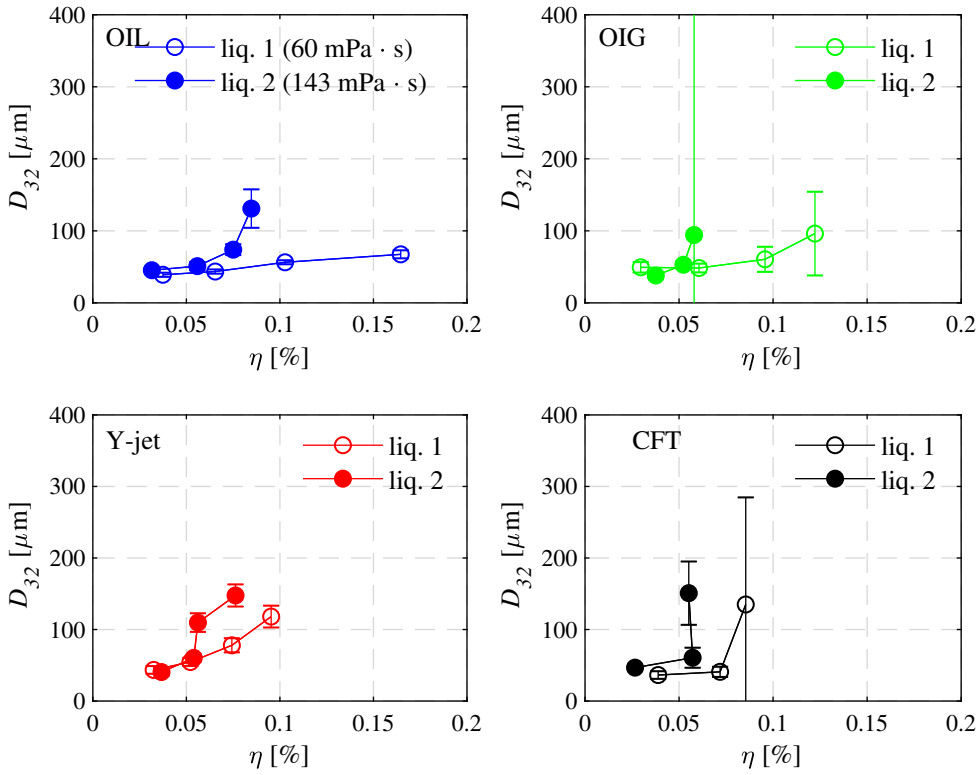

Figure 13. Atomization efficiency and drop sizes.

6. Overall Assessment of the Atomizers

As a variety of analyses were provided to show the differences between the work of the atomizers, we summarize some of the most significant observations in the following table to provide the reader with a complex view of our results (Table 9). The nozzles were evaluated in 5 categories by grades within a range from 1 (best) to 4 (worst). The "X" indicates where a comparison could not be performed.

The presented comparison shows the qualitative dependency of the design parameters of the nozzles (mixing chamber and discharge orifice dimensions, liquid injection), spray quality and spraying

efficiency. It can be stated that the best performance will be achieved by a well-designed nozzle with a wall-attached internal flow pattern and sudden acceleration at the discharge orifice (OIL). On the other hand, however, this design shows a sensitivity on liquid viscosity. In applications where liquid viscosity cannot be constantly maintained, a nozzle with fast internal flow (Y-jet) provides stable spray quality.

Table 9. Overall rating of our atomizers for spraying at low GLRs.

					Sensitivity to μ_l	
Atomizer	**Low GLRs Performance**	D_{32}	**Pulsations**	η	D_{32}	η
OIL	1	1	2	1	2	3
OIG	X	2	3	2	X	X
Y-jet	1	2	1	3	1	2
CFT	X	3	4	4	X	X

7. Conclusions

We examined four atomizers, spraying two highly viscous liquids with a set of operating conditions to provide a comparison of their spraying abilities in order to define the advantages, disadvantages and potential applications for the spraying of liquid fuels. The comparison criteria were chosen to highlight the atomizers' differences in two areas: spray quality and the efficiency of work.

The time-averaged D_{32} was comparable for all the tested devices for GLR $\geq$ 10%. Also, the spray pulsations were weak, which led to small variations in drop size. Good spray quality was provided by high pressurized gas consumption, which led to low atomization efficiency for all the nozzles ($\eta \leq 0.06\%$).

An analysis of the time-resolved spray behavior documents that the nozzle designs based on the liquid injected to the gas stream (OIL and Y-jet atomizers) featured low spray pulsations, narrow drop size range and acceptable spraying efficiency. Their internal flows were characterized with wall-attached liquid stream even at low-GLR regimes.

Switching of the fluid injection ports from OIL to the OIG nozzle configuration led to internal flow with the presence of large gas and liquid structures, which caused local GLR fluctuations in the discharge orifice, along with spray pulsations. It resulted in large drops present in the spray, generated by the random discharge of the liquid that was not properly mixed with the pressurized air.

The OIL nozzle has shown to have a very good spraying ability in comparison to its OIG counterpart. It was caused by the fact that the injected liquid was immediately attached to the mixing chamber wall without a chance to interact with the gas core (as it did in the OIG atomizer). The simple design change influenced fluid-mixing mechanism so the annular flow was able to form even with low gas consumption. The working principle of the OIL nozzle differs from the original effervescent atomizer design (OIG) so much that it can be considered to be a separated atomizer type.

This device is characteristic by the stable operation and high efficiency when working with the liquid of constant viscosity. It is a good alternative of the currently used OIG nozzles which are often used for injection of fuel to the gas turbines or industrial furnaces.

The main advantage of the Y-jet atomizer was relative low sensitivity of the spray quality on the liquid viscosity. It provided stable performance with a narrow drop sizes spectrum and acceptable mean drop size. It is currently widely used in the industrial furnaces, but the observed behavior allows use of this nozzle in applications, where the liquid viscosity oscillates, such as spray-drying of the liquids in the food-processing industry.

The CFT nozzle, however, although giving the finest spray with the less viscous liquid at GLR = 20%, performed poorly in low gas consumption regimes and its usage potential at the atomization of the viscous fuel is low. Its potential lies in the other applications, where low gas consumption and high viscosity of the liquid are not required but the very fine spray is needed.

One interesting secondary finding is that for the OIG device the Golan and Stenning two-phase flow map predicted an annular flow for all of the tested working regimes which was not in accordance with the observed spray behavior, especially at low GLRS. The other tested flow map (Baker, Barnea) provided acceptable results, although the internal flow pattern estimation had to be supported by the additional dimensionless parameters to satisfactorily explain the OIG nozzle spray behavior.

Author Contributions: M.M.: Funding acquisition, Investigation, Methodology, Visualization, Writing—original draft, Writing—review and editing. J.J.: Funding acquisition, Project administration, Writing—review and editing. H.P.K.: Resources. V.G.: Resources, Writing—review and editing. All authors have read and agreed to the published version of the manuscript.

Funding: The authors acknowledge the financial support from the project No. 18-15839S funded by the Czech Science Foundation, the project "Computer Simulations for Effective Low-Emission Energy Engineering" funded as project No. CZ.02.1.01/0.0/0.0/16 026/0008392 by Operational Programme Research, Development and Education, Priority axis 1: Strengthening capacity for high-quality research and the project LTAIN19044 funded from the program INTER-EXCELLENCE by the Ministry of Education, Youth and Sports of the Czech Republic.

Conflicts of Interest: The authors declare no conflict of interest.

References

1. Jedelsky, J.; Jicha, M. Energy conversion during effervescent atomization. *Fuel* **2013**, *111*, 836–844. [CrossRef]
2. Sovani, S.; Sojka, P.; Lefebvre, A. Effervescent atomization. *Prog. Energy Combust. Sci.* **2001**, *27*, 483–521. [CrossRef]
3. Ferreira, G.; Garcia, J.; Barreras, F.; Lozano, A.; Lincheta, E. Design optimization of twin-fluid atomizers with an internal mixing chamber for heavy fuel oils. *Fuel Process. Technol.* **2009**, *90*, 270–278. [CrossRef]
4. Buckner, H.N.; Sojka, P.E.; Lefebvre, A.H. Effervescent Atomization of Coal-Water Slurries. *ASME Publ. Pet. Div.* **1990**, *30*, 105–108.
5. Daviault, S.G.; Ramadan, O.B.; Matida, E.A.; Hughes, P.M.; Hughes, R. Atomization performance of petroleum coke and coal water slurries from a twin fluid atomizer. *Fuel* **2012**, *98*, 183–193. [CrossRef]
6. Broniarz-Press, L.; Ochowiak, M.; Woziwodzki, S. Atomization of PEO aqueous solutions in effervescent atomizers. *Int. J. Heat Fluid Flow* **2010**, *31*, 651–658. [CrossRef]
7. Broniarz-Press, L.; Ochowiak, M.; Rozanski, J.; Woziwodzki, S. The atomization of water–oil emulsions. *Exp. Therm. Fluid Sci.* **2009**, *33*, 955–962. [CrossRef]
8. Schroeder, J.; Kleinhans, A.; Serfert, Y.; Drusch, S.; Schuchmann, H.P.; Gaukel, V. Viscosity ratio: A key factor for control of oil drop size distribution in effervescent atomization of oil-in-water emulsions. *J. Food Eng.* **2012**, *111*, 265–271. [CrossRef]
9. Schroeder, J.; Kraus, S.; Rocha, B.B.; Gaukel, V.; Schuchmann, H.P. Characterization of gelatinized corn starch suspensions and resulting drop size distributions after effervescent atomization. *J. Food Eng.* **2011**, *105*, 656–662. [CrossRef]
10. Staehle, P.; Schuchmann, H.P.; Gaukel, V. Performance and Efficiency of Pressure-Swirl and Twin-Fluid Nozzles Spraying Food Liquids with Varying Viscosity. *J. Food Process. Eng.* **2015**. [CrossRef]
11. Alvim, I.D.; Stein, M.A.; Koury, I.P.; Dantas, F.B.H.; de Camargo Vianna Cruz, C.L. Comparison between the spray drying and spray chilling microparticles contain ascorbic acid in a baked product application. *LWT-Food Sci. Technol.* **2016**, *65*, 689–694. [CrossRef]
12. Yu, H.; Teo, J.; Chew, J.W.; Hadinoto, K. Dry powder inhaler formulation of high-payload antibiotic nanoparticle complex intended for bronchiectasis therapy: Spray drying versus spray freeze drying preparation. *Int. J. Pharm.* **2016**, *499*, 38–46. [CrossRef] [PubMed]
13. Huang, X.; Wang, X.; Liao, G. Characterization of an effervescent atomization water mist nozzle and its fire suppression tests. *Proc. Combust. Inst.* **2011**, *33*, 2573–2579. [CrossRef]
14. Chin, J.; Lefebvre, A. A design procedure for effervescent atomizers. *J. Eng. Gas Turbines Power* **1995**, *117*, 266–271. [CrossRef]
15. Loercher, M.; Schmidt F.; Mewes, D. Flow field and phase distribution inside effervescent atomizers. In Proceedings of the 9th ICLASS, Sorrento, Italy, 13–17 July 2003.
16. Zaremba, M.; Weiß, L.; Maly, M.; Wensing, M.; Jedelsky, J.; Jicha, M. Low-pressure twin-fluid atomization: Effect of mixing process on spray formation. *Int. J. Multiph. Flow* **2017**, *89*, 277–289. [CrossRef]

17. Baker, O. Simultaneous Flow of Oil and Gas. *Oil Gas J.* **1954**, *53*, 185–195.
18. Golan L. P, S.A.H. Two-Phase Vertical Flow Maps. *Proc. Inst. Mech. Eng.* **1969**, *184*, 108–114. [CrossRef]
19. Barnea, D.; Shoham, O.; Taitel, Y. Flow pattern transition for downward inclined two phase flow; horizontal to vertical. *Chem. Eng. Sci.* **1982**, *37*, 735–740. [CrossRef]
20. Song, S.; Lee, S. Study of atomization mechanism of gas/liquid mixtures flowing through Y-jet atomizers. *At. Sprays* **1996**, *6*, 193–209. [CrossRef]
21. Mlkvik, M.; Stähle, P.; Schuchmann, H.; Gaukel, V.; Jedelsky, J.; Jicha, M. Twin-fluid atomization of viscous liquids: The effect of atomizer construction on breakup process, spray stability and droplet size. *Int. J. Multiph. Flow* **2015**, *77*, 19–31. [CrossRef]
22. Zaremba, M.; Kozak, J.; Maly, M.; Weiß, L.; Rudolf, P.; Jedelsky, J.; Jicha, M. An experimental analysis of the spraying processes in improved design of effervescent atomizer. *Int. J. Multiph. Flow* **2018**, *103*, 1–15. [CrossRef]
23. Panão, M.; Moreira, A. Thermo- and fluid dynamics characterization of spray cooling with pulsed sprays. *Exp. Therm. Fluid Sci.* **2005**, *30*, 79–96. [CrossRef]
24. Pacifico, A.L.; Yanagihara, J.I. The influence of geometrical and operational parameters on Y-jet atomizers performance. *J. Braz. Soc. Mech. Sci. Eng.* **2014**, *36*, 13–22. [CrossRef]
25. Pougatch, K.; Salcudean, M.; McMillan, J. Influence of mixture non-uniformity on the performance of an effervescent nozzle. *Fuel* **2014**, *116*, 601–607. [CrossRef]
26. Gottlieb, N.; Schwartzbach, C. Development of an internal mixing two-fluid nozzle by systematic variation of internal parts. In Proceedings of the 19th ILASS Europe, Nottingham, UK, 6–8 September 2004.
27. Kleinhans, A.; Georgieva, K.; Wagner, M.; Gaukel, V.; Schuchmann, H.P. On the characterization of spray unsteadiness and its influence on oil drop breakup during effervescent atomization. *Chem. Eng. Process. Process Intensif.* **2016**, *104*, 212–218. [CrossRef]
28. Wittner, M.O.; Karbstein, H.P.; Gaukel, V. Spray performance and steadiness of an effervescent atomizer and an air-core-liquid-ring atomizer for application in spray drying processes of highly concentrated feeds. *Chem. Eng. Process. Process Intensif.* **2018**, *128*, 96–102. [CrossRef]
29. Mullinger, P.; Chigier, N. The design and performance of internal mixing multijet twin fluid atomizers. *J. Inst. Fuel* **1974**, *47*, 251–261.
30. Lefebvre, A.H. A novel method of atomization with potential gas turbine applications. *Def. Sci. J.* **1988**, *38*, 353–362. [CrossRef]
31. Chin, J. Effervescent Atomization and Internal Mixing Air Assist Atomization. *Int. J. Turbo Jet Engines* **1995**, *12*, 119–128. [CrossRef]
32. Ferreira M. Teixeira, F. Bates, J.B.J. Detailed investigation of the influence of fluid viscosity on the performance characteristics of plain-orifice effervescent atomizers. *At. Sprays* **2001**, *11*, 107–124.
33. Tamaki, N.; Shimizu, M.; Hiroyasu, H. *Atomization of High Viscous Liquid Jet by Internal Mixing Twin-Fluid Atomizer*; ILASS Europe: Nottingham, UK, 2004.
34. Jedelsky, J. Two-Phase Flow Regime Determination Version 1.2c. 2014. Available online: http://two-phase-flow.ic.cz/ (accessed on 29 July 2020).
35. Jedelsky, J. Calculation of Two-Phase Discharge. 2014. Available online: http://two-phase-flow.ic.cz/ (accessed on 29 July 2020).
36. Arai, T.; Hashimoto, H. Disintegration of Thin Liquid Sheet in Cocurrent Gas Stream: Wave Motion of Thin Liquid Sheet and Breakup Patterns. *Trans. Jpn. Soc. Mech. Eng. Ser. B* **1985**, *51*, 3336–3343. [CrossRef]
37. Wittner, M.; Ballesteros, M.; Link, F.; Karbstein, H.; Gaukel, V. Air-core-liquid-ring (ACLR) atomization part II: Influence of process parameters on the stability of internal liquid film thickness and resulting spray droplet sizes. *Processes* **2019**, *7*, 616. [CrossRef]
38. Faeth, G.; Hsiang, L.P.; Wu, P.K. Structure and breakup properties of sprays. Annual Reviews in Multiphase Flow 1995. *Int. J. Multiph. Flow* **1995**, *21*, 99–127. [CrossRef]
39. Jicha, M.; Jedelsky, J. Unsteadiness in effervescent sprays: A new evaluation method and the influence of operational conditions. *At. Sprays* **2008**, *18*, 49–83. [CrossRef]